INTERFACIAL SURFACE ENERGIES – STAINLESS STEEL AND TITANIUM NITRIDE SUBSTRATES WITH $CaCO_3$ AND $CaHPO_4$ DEPOSITIONS

***E. Puhakka[1], U. Ojaniemi[2] and T. Pättikangas[2]**
[1] Department of Chemistry, P.O. Box 55, FI-00014 UNIVERSITY OF HELSINKI, Finland
[2] VTT Technical Research Centre of Finland Ltd, P.O. Box 1000, FI-02044 VTT, Finland

ABSTRACT

In order to control fouling of heat transfer units, it is significant if deposition formation can be predicted beforehand. For this purpose, multiphase computational fluid dynamics simulations are very useful, because surface properties of heat transfer materials, properties of depositions and process parameters can be taken into account in the simulations. In order to increase the accuracy of the results, molecular modelling was used to calculate interfacial surface energies between substrates and depositions. The focus was on the stainless steel surfaces and titanium nitride coated surfaces which are exposed to calcium carbonate and calcium phosphate depositions in dairy industry. Determination of the interfacial energies are based on the calculated free surface energies of materials which are very laborious to determine experimentally. In the present research, free surface energies were calculated for Cr/CrFe oxides and TiN substrates and $CaCO_3$ and $CaHPO_4$ depositions including work of adhesion values. As a result, detailed fouling mechanisms with energetics and interfacial energies were obtained.

INTRODUCTION

Deposition formation of unwanted material on heat transfer surfaces, i.e. fouling, is a significant factor which decreases the energy efficiency of process equipment and thus has a marked effect on carbon dioxide (CO_2) releases and thus on climate change. In dairy processes also product quality is deteriorated due to reduction in proper heating.

Fouling in dairy processes has been widely studied. The chemistry of fouling from milk fluids is qualitatively understood, and mathematical models in low temperature exist. However, the behaviour of the systems at ultrahigh temperature (UHT) processing, where the inorganic deposits also take place is still not clearly understood (Sadeghinezhad et al., 2013). In milk fouling deposits, calcium phosphate and whey protein (β-Lg) are the major components. Due to their heat sensitivity, both these components form insoluble aggregates in bulk solution. At relatively high temperatures (above 85 °C), the main deposit is calcium phosphate (Sadeghinezhad et al., 2013).

In dairy and other food processing industries, plate heat exchangers are widely applied. Fouling depends on several surface properties like roughness, surface composition and surface energy. Therefore, modified surface materials have also been of special interest (polishing, patterning and coating) in order to prevent initiation of fouling.

The fouling models for fouling process presented in literature are most often based on mass transfer on the surface or on a surface reaction. The modelling of adhesion on the surface has gained less attention, though the fouling process is generally accepted to be affected by surface properties.

A prerequisite for a development of materials and controlling heating/cooling processes is that the adhesion mechanisms of depositions onto surfaces are known. Generally fouling mechanisms are classified into six groups: crystallization, particle attachment, chemical fouling, corrosion, biological fouling and solidification (Bott, 1995; Mwaba et al., 2006). The fouling rate, the chemical composition and the physical properties of deposited material on the surfaces depend on process conditions (e.g. pH, temperature, concentrations of soluble species of particles, fluid flow) and construction materials of heat transfer surfaces (Kostoglou and Karabelas, 1998).

In dairy processes surface modification toward low total surface energy has been reported to be an appropriate approach of fouling mitigation. However, it is demanding to gather information about interaction mechanisms (chemical or physical) between heat transfer surfaces and depositions with experimental methods. Therefore, modelling techniques should be useful, and of these Computational Fluid Dynamics (CFD) method is suitable one. However, there is not available a CFD model for particulate fouling in dairy processes which could take into account the surface properties of the materials, although the importance of the surface energies is highlighted (Sadeghinezhad et al., 2013). Such a model can be applied in predicting the likely profile of milk

ISBN: 978-0-9984188-1-0; Published online www.heatexchanger-fouling.com

deposition, and in designing the plate shape, corrugation profile and surface materials in order to reduce the costs due to fouling.

In these CFD models, interfacial surface energy values are needed which can be defined using free surface energies of materials. The free surface energies are very laborious to determine experimentally or the measurements do not give sufficiently consistent values to be used in modelling work. However, molecular modelling is a proven technique to calculate the free surface energies theoretically.

Now, the deposition formation and surface energy values for calcium phosphate on the stainless steel surfaces was defined. The results were compared to our earlier results for calcium carbonate (Puhakka and Lecoq, 2015). In addition to the stainless steel, titanium nitride (TiN) coating material was also considered. The investigated coating was selected based on industrial interest, when mitigation of fouling is attempted on heat transfer surfaces.

METHODS

Density functional methods were used to investigate surface oxide layer structures of stainless steel, titanium nitride coating, and $CaHPO_4$ and $CaCO_3$ depositions formation on these surfaces. Because real surfaces are subject to the effect of ambient process conditions, the role of process fluid (water) for surface structures was taken into account. Therefore, the adsorption mechanism of water onto the surfaces was investigated, and thereafter the model surfaces for deposition formation studies were generated. All the calculations were performed with the CASTEP (CAmbridge serial total energy package) code implemented into Materials Studio versions 8.0 (Dassault Systemès, 2014) and BIOVIA Materials Studio 2017 *R2* (Dassault Systemès, 2016). In the calculations, the total electronic energy and overall electronic density distribution were solved in order to define the energetically stable structures for surfaces and adsorbates on the surfaces (Leach, 2001).

During the geometry optimization of the structures of stainless steel and TiN coating, and adsorption studies of water and calcium (Ca^{2+}), diphosphate (HPO_4^{2-}) and carbonate (CO_3^{2-}) ions onto the surfaces, the exchange-correlation was described with generalized gradient approximation GGA-PBE. As a compromise between the accuracy and computational time of calculations, the ultrasoft pseudopotentials were used. In the potential of chromium, iron and titanium, the semicore states were treated as a part of the core. The used potentials were C_00PBE.usp for carbon, Ca_00PBE.usp for calcium, Cr_00PBE.uspcc for chromium, Fe_00PBE.uspcc for iron, H_00PBE.usp for hydrogen, N_00PBE.usp for nitrogen, O_soft00.usp for oxygen, and Ti_00.uspcc for titanium. The kinetic cut-off energy for a plane wave expansion of the wave function was 280 eV.

Energy values for the formation of $CaCO_3$ depositions were calculated from the single-point energies of the ions and the surface structures with and without the adsorbed ions. The calculations were performed using the GGA-RPBE exchange-correlation, and the kinetic cut-off energy was 330 eV.

Interfacial free energies, surface energies between two materials can be calculated:

$$\gamma_{12} = \gamma_1 + \gamma_2 + w_{ad} \quad (1)$$

where w_{ad} is the work of adhesion. The work of adhesion was calculated according to the following equation:

$$w_{ad} = (E_1 + E_2 - E_{12}) / A \quad (2)$$

where E_1 and E_2 are the energies of the separated materials and E_{12} is the energy of the complete model, and A is surface area of the model (Hölck et al., 2011). The same structures which were used to calculate deposition formation energies were utilized. Only one interface is needed to take into account, because 3D periodic models with vacuum layer were used.

Surface energies, γ_1 and γ_2, can be calculated according to the following equation:

$$\gamma_{surf} = [E_{surf} - (n_{surf}/n_{bulk})E_{bulk}] / 2A \quad (3)$$

where γ_{surf} is the surface energy of a surface slab, E_{surf} is the energy of the surface slab, n_{surf} is the number of atoms in the surface slab, n_{bulk} is the number of atoms in the bulk, E_{bulk} is the energy of the bulk, and A is the surface area of the surface slab.

The quality of the surface calculations depends on the number of atomic layers and the thickness of a vacuum layer used in a supercell.

RESULTS AND DISCUSSION

Chromium/Iron (Cr_xFe_y) Oxides

The properties of stainless steel are based on the passive layer on the surface, which mainly consists of chromium oxides and has a thickness of about ten molecular layers (Pießlinger-Schweiger, 2005). Therefore, in our earlier molecular modelling study, the chromium-rich oxide layer of stainless steel was described by the hexagonal Cr_2O_3, the optimized lattice parameters of which are a = b = 513.8 pm, c = 1403.6 pm and c/a = 2.732 (Puhakka et al., 2008). Further, the effect of the iron content on the surface structure of the corrosion protective Cr-rich oxide layer was

ISBN: 978-0-9984188-1-0; Published online www.heatexchanger-fouling.com

considered (Puhakka and Lecoq, 2015). After the pure Cr_2O_3 structure was determined, then also the mixed Cr_xFe_y oxides was studied. It was supposed that Cr_xFe_y oxides have the same kind crystalline structure than the pure Cr_2O_3 has. In Table 1, lattice parameters for hexagonal Cr_2O_3 and Fe_2O_3, and three tetragonal $Cr_8Fe_4O_{18}$ structures are shown. In the $Cr_8Fe_4O_{18}$ oxides, the substitution of Fe atoms was made for different lattice points. Of these structures, two $Cr_8Fe_4O_{18}$ oxides were selected to the present studies (Fig. 1).

Earlier (Puhakka *et al.*, 2008), the fully oxided (004) surface of Cr_2O_3 was supposed to describe the surface structure of stainless steel. However, XPS analyses of stainless steel surface highlighted the presence of metallic chromium, Cr_2O_3 and $Cr(OH)_3$. This is consistent with literature data (Diawara, 2012), that the uppermost layer of stainless steel consists of Cr-$(OH)_3$ groups. Therefore, the (006) surface with three-coordinated Cr atoms was selected for our studies. On this surface, the vacant sites of Cr atom were occupied with hydroxide groups, and the surface structure was optimized in order to obtain energetically stable structures for deposition formation studies.

Table 1. Lattice parameters of Cr_xFe_y oxides.

Material	Exptl. values (pm)		Calculated values (pm)	
	a = b	c	a = b	c
Fe_2O_3	503.5	1 372.0	n/a	n/a
Cr_2O_3	495.9	1 359.3	513.8	1 403.6
$Cr_8Fe_4O_{18}$(I)			503.3	1 373.1
$Cr_8Fe_4O_{18}$(II)			504.8	1 370.4
$Cr_8Fe_4O_{18}$(III)			513.3[a]	1 392.4

[a] Typographical error in the reference of Puhakka and Lecoq (2015) corrected.

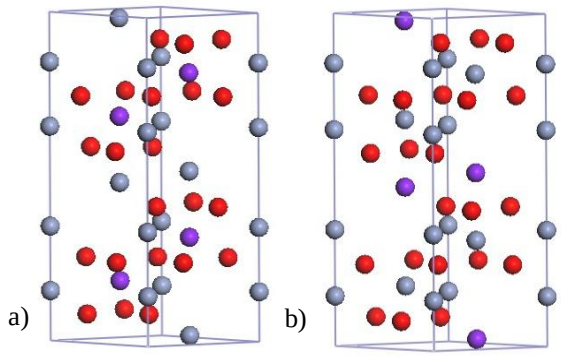

Fig. 1. The unit cells of Cr_xFe_y oxides: a) $Cr_8Fe_4O_{18}$ (I) and b) $Cr_8Fe_4O_{18}$ (III). Red spheres: oxygen. Grayish blue spheres: chromium. Blue spheres: iron.

Titanium nitride

TiN was considered as coating material for stainless steel to mitigate deposition formation. TiN exists in cubic crystal structure. The optimized lattice parameters of TiN are a = b = c = 430.0 pm. The unit cell together with morphology is shown in Fig. 2. Of TiN surfaces, the (111) and (200) surfaces are the most dominant. On the (111) surface, the Ti atoms are on the upper-most layer, and on the (200) surface, the nitrogen atoms (Fig. 3).

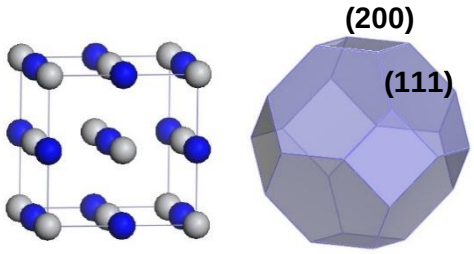

Fig. 2. TiN: the unit cell (left) and morphology (right). Light blue spheres: titanium. Blue spheres: nitrogen.

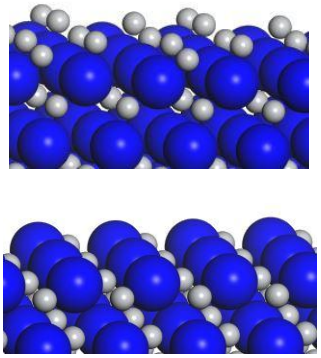

Fig. 3. TiN surfaces: the (111) surface (upper) and the (200) surface (below).

Deposition Formation on the Surfaces

In the $CaCO_3$ and $CaHPO_4$ deposition formation studies, the initiation of crystallization fouling caused by Ca^{2+}, CO_3^{2-} and HPO_4^{2-} species was investigated both on the Cr_xFe_y oxide and TiN surfaces. The study was performed by determining the adsorption positions and energies of a Ca^{2+} ion on the surfaces, and after that CO_3^{2-} or HPO_4^{2-} ions were adsorbed onto the Ca^{2+} covered surfaces. By optimizing the positions of Ca^{2+} and CO_3^{2-} or HPO_4^{2-} on the surfaces at the same time, the bonding geometry of $CaCO_3$ or $CaHPO_4$ on the surface was achieved. In the case of TiN, it was also studied depositions where the ions adsorb first and the cations secondly. As a result, the detailed reaction mechanisms with energetics were obtained for the formation of $CaCO_3$ and $CaHPO_4$ depositions.

In our earlier studies (Puhakka *et al.*, 2008), the deposition formation energies were determined

ISBN: 978-0-9984188-1-0; Published online www.heatexchanger-fouling.com

for $CaCO_3$ on the $Cr(OH)_3$ surface, and two types of $CrFe(OH)_3$ surfaces. In the case of $CrFe(OH)_3$ surfaces, either Cr atoms or Fe atom are on the uppermost surface. The deposition formation energies are -1.03 eV, -2.16 eV and -4.04 eV, respectively. The coverage of the deposition on the surface is high, and the layer of the deposition is very dense (Fig. 4).

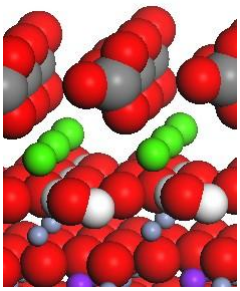

Fig. 4. $CaCO_3$ deposition on the $CrFe(OH)_3$ (I) surface where Cr atoms are upper than Fe atoms. Red spheres: oxygen. Greyish blue spheres: chromium. Blue spheres: iron. White spheres: hydrogen. Green spheres: calcium. Grey spheres: carbon.

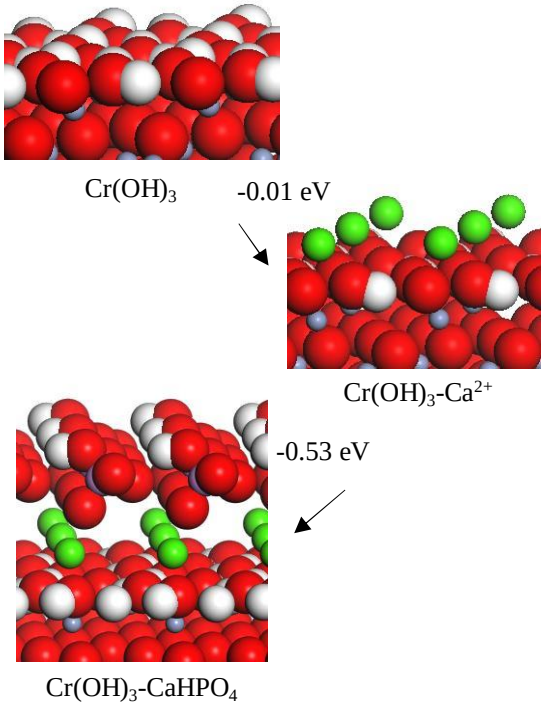

Fig. 5. $CaHPO_4$ deposition on the $Cr(OH)_3$ surface. Red spheres: oxygen. Greyish blue spheres: chromium. White spheres: hydrogen. Green spheres: calcium. Blue spheres: phosphate.

In Fig. 5, the $CaHPO_4$ deposition formation on the $Cr(OH)_3$ surface is shown, and the released energy is -0.54 eV. The deposition layer is very similar than in the case of $CaCO_3$ depositions (Fig. 4).

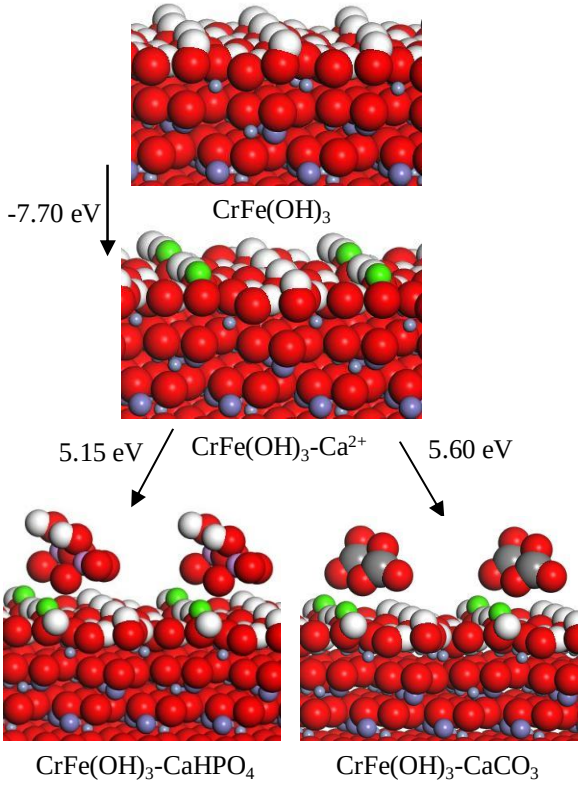

Fig. 6. $CaHPO_4$ and $CaCO_3$ deposition on the $CrFe(OH)_3$ surface.

In the case of $CrFe(OH)_3$ surfaces, the $CaHPO_4$ does not form as dense depositions as on the $Cr(OH)_3$ surfaces (Fig. 6). The coverage of the energetically stable deposition layers is only about one quarter of the coverage on the $Cr(OH)_3$ surface. The deposition formation energies are -2.55 eV for $CaHPO_4$ deposition and -2.10 eV for $CaCO_3$ deposition (-2.16 eV for the dense coverage for $CaCO_3$). It seems that the deposition formation energies are not dependent on the coverage degree on the surface.

In Figs. 7 and 8, the deposition formation mechanisms for $CaHPO_4$ and $CaCO_3$ depositions are presented on the (200) and (111) surfaces. It was considered that the deposition formation can start either via the adsorption of cations or anions (Fig. 7). The cations adsorb strongly onto the (200) surface, and the anions repel the bonding. The interaction of CO_3^{2-} and HPO_4^{2-} with the surface is very similar. However, if the deposition formation can start via the adsorption of anions, then the deposition is more tightly bonded onto the surface than if the deposition formation starts via the adsorption of cations. The $CaHPO_4$ depositions are more tightly bonded onto the surface than the $CaCO_3$ depositions.

In Fig. 8, the deposition formation mechanisms for $CaHPO_4$ and $CaCO_3$ depositions are presented on the (111) surface. On this surface, the formation energies released during the deposition formation are significantly larger than

ISBN: 978-0-9984188-1-0; Published online www.heatexchanger-fouling.com

on the (200) surface. Also, on this surface, the $CaHPO_4$ depositions are more tightly bonded onto the surface than the $CaCO_3$ depositions.

Work of adhesion

The same structures which were used to calculate deposition formation energies were utilized to calculate the work of adhesion, w_{ad}, for $CaCO_3$ and $CaHPO_4$ depositions on the Cr_2O_3, $Cr(OH)_3$, $CrFe(OH)_3$ and TiN surfaces. The results are shown in Table 2.

The work of adhesion is the strongest, 4.4 - 4.6 J/m^2 on the $Cr(OH)_3$ surfaces because of the strong hydrogen bonding. On the $Cr(OH)_3$ surfaces, the deposition layer is also very dense. On the other surfaces, the coverage degree of the stable deposition layer varies from 0.25 to 0.75, and the work of adhesion from 0.6 – 1.4 J/m^2. There are no significant differences between $CaCO_3$ and $CaHPO_4$ depositions.

Surface energies

Surface energies between two materials were calculated according to Equation 1. First, surface energies of pure materials were determined according to Equation 2. The quality of the surface energy calculation depends on the number of atomic layers, and the number of the layers is enough when the value of the surface energy converges achieving a stable level. In some cases, the effect of the size of the surface area on the surface energy values was also tested.

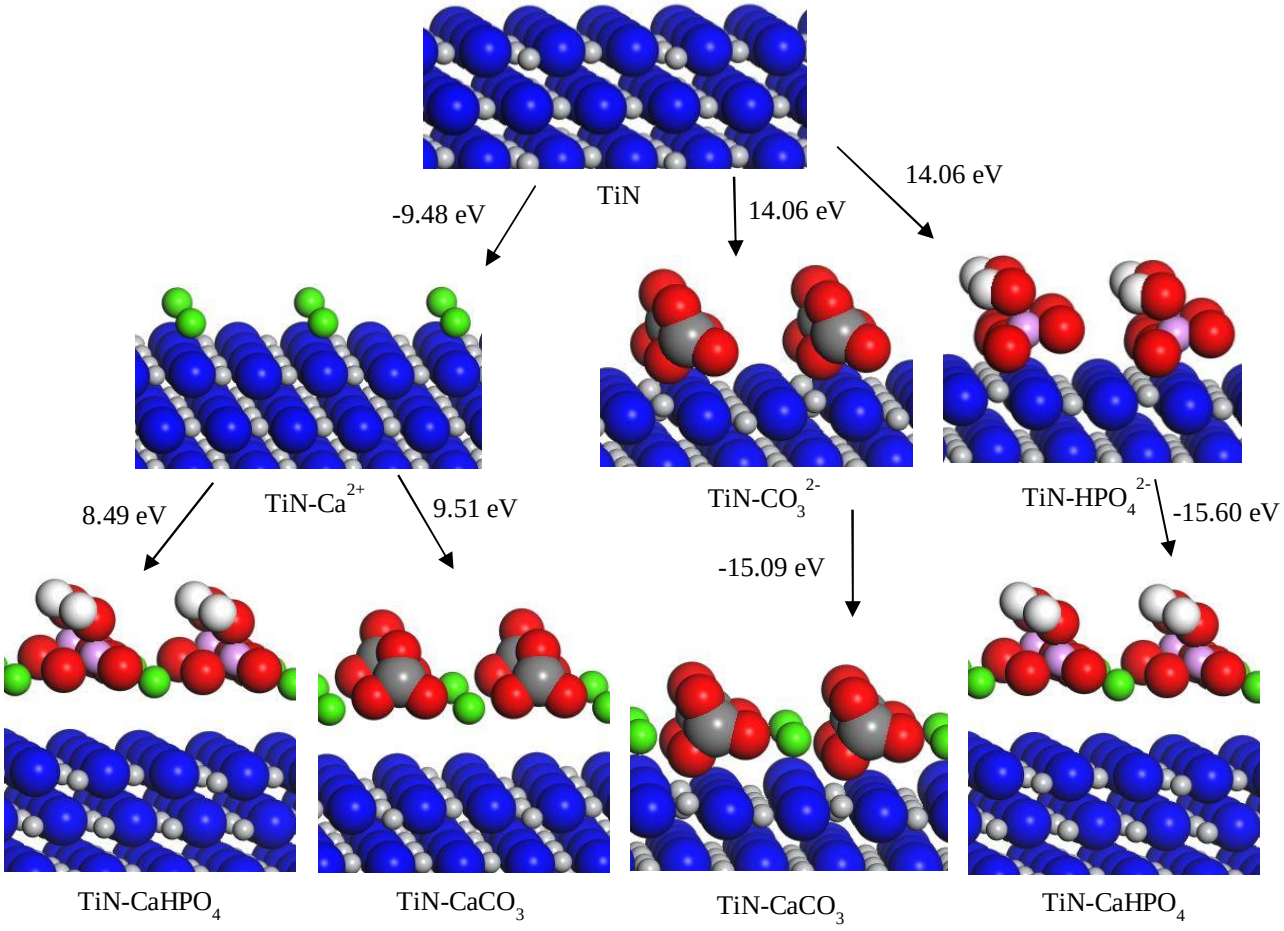

Fig. 7. $CaHPO_4$ and $CaCO_3$ depositions on the TiN (200) surface. The deposition formation energies from left to right are -0.99 eV, 0.03 eV, -1.03 eV and -1.54 eV.

ISBN: 978-0-9984188-1-0; Published online www.heatexchanger-fouling.com

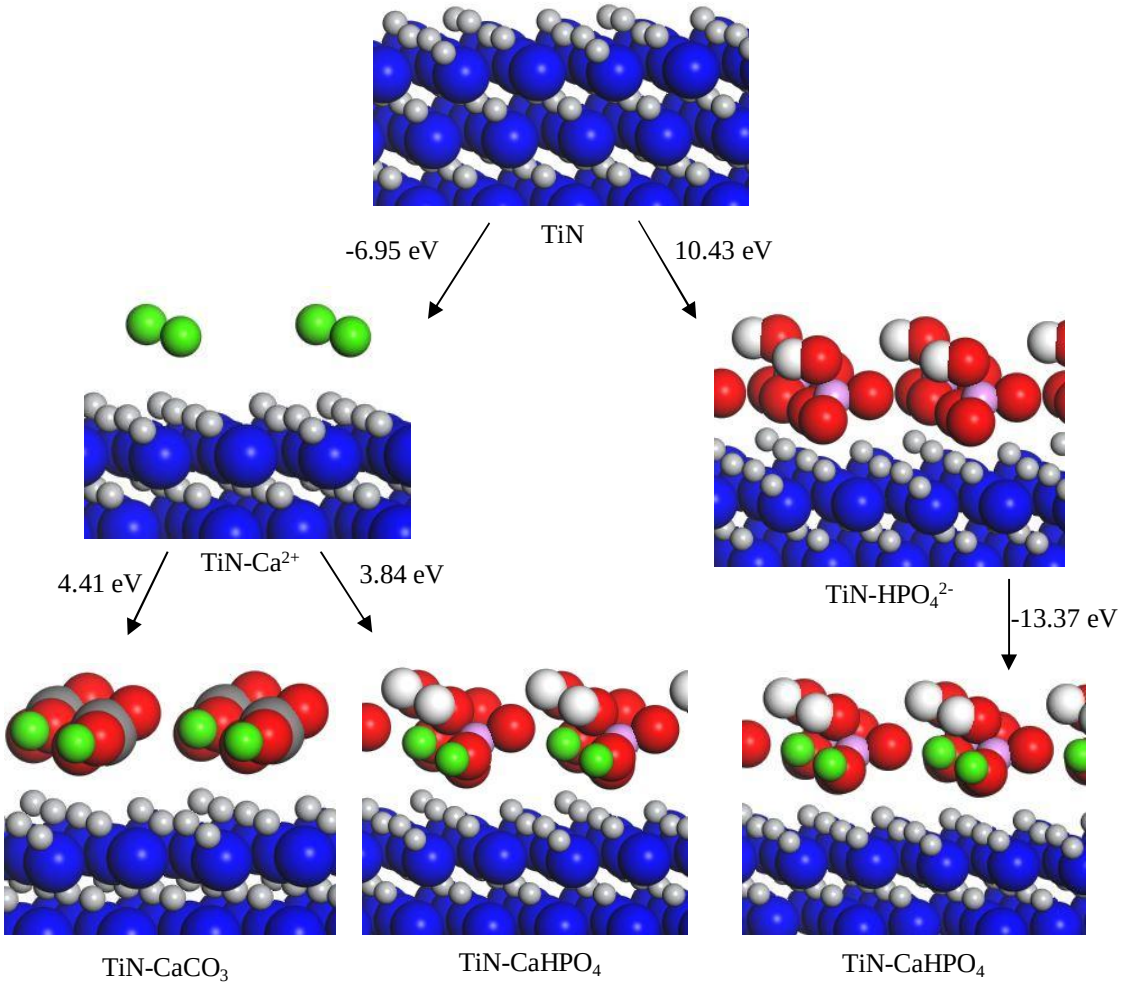

Fig. 8. $CaHPO_4$ and $CaCO_3$ depositions on the TiN (111) surface. The deposition formation energies from left to right are -2.54 eV, -3.11 eV and -2.94 eV.

In Fig. 9, the calculated surface energies of pure materials are shown as a function of the thickness of surface layer. The results show that the surface energies of CaCO3 and CaHPO4 depositions and CrFe oxide and TiN surface materials reach the stable level at rather low thickness values. On the other hand, pure chromium oxide does not stabilize with the used models.

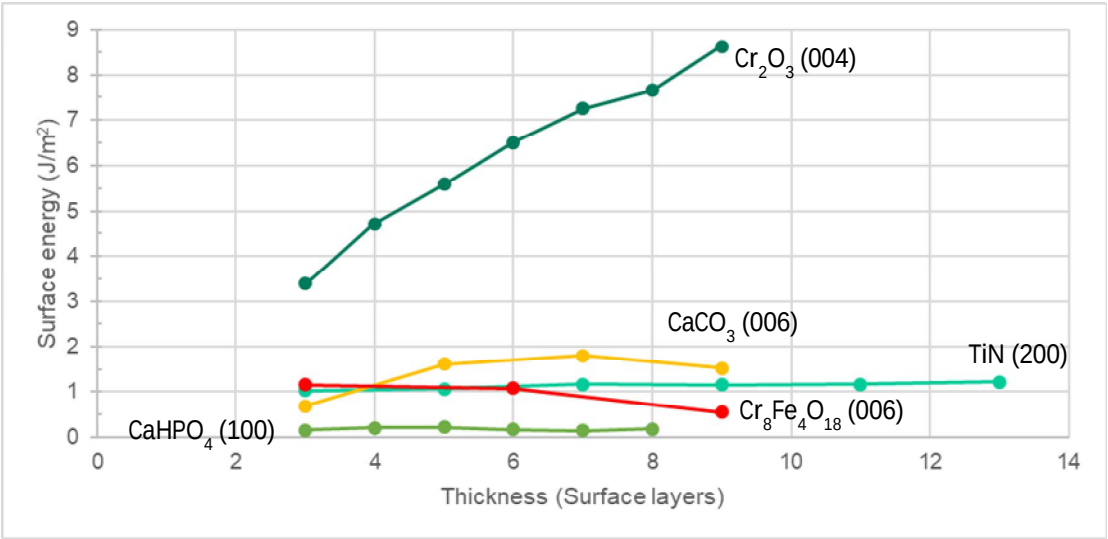

Fig. 9. The calculated surface energies of pure materials as a function of the thickness of surface layers.

ISBN: 978-0-9984188-1-0; Published online www.heatexchanger-fouling.com

Table 2. The surface energies γ_1 for substrates, the surface energies γ_2 for depositions, the coverage of the depositions on the surface, the work of adhesion w_{ad} and the interfacial energies γ_{12}.

Substrate	γ_1 (J/m^2)	Deposition	γ_2 (J/m^2)	Coverage	w_{ad} (J/m^2)	γ_{12} (J/m^2)
Cr_2O_3	7.7	$CaCO_3$	1.6	~ 0.25	1.1	8.2
		$CaHPO_4$	0.2	~ 0.25	1.1	6.8
$Cr(OH)_3$	8.7	$CaCO_3$	1.6	~ 1	4.4	5.9
		$CaHPO_4$	0.2	~ 1	4.6	4.3
$CrFe(OH)_3$	3.8	$CaCO_3$	1.6	~ 0.25	1.1	4.3
		$CaHPO_4$	0.2	~ 0.25	1.4	2.6
TiN	1.2	$CaCO_3$	1.6	~ 0.5	0.8	2.0
		$CaHPO_4$	0.2	~ 0.75	0.6	0.8

When the surface energies for pure materials and the work of adhesion between the substrates and depositions are available, then the interfacial energies can be calculated. The results are shown in Table 2. The interfacial energies are systematically minor for $CaHPO_4$ depositions than for $CaCO_3$ depositions.

CONCLUSIONS

The present study indicated that the determination of the interfacial energies is possible using the calculated free surface energies of materials. When the structure of material at the atomic level is very symmetrical, and the repeatable surface structure is similar as the repeatable bulk structure, then the interfacial energies are obtained rather reliably.

ACKNOWLEDGEMENTS

The research leading to these results has received funding from Academy of Finland under grant agreement no. 298404.

NOMENCLATURE

CASTEP	CAmbridge Serial Total Energy Package
GGA-PBE	Perdew, Burke and Ernzerhof version of generalized gradient approximation functional
GGA-RPBE	Hammer, Hansen, Norskov modified Perdew, Burke and Ernzerhof version of generalized gradient approximation
XRD	X-Ray Diffraction

REFERENCES

Bott, T. R., 1995, *Fouling of Heat Exchangers*, Elsevier, Amsterdam.

Dassault Systemès, 2016, *BIOVIA Materials Studio 2017 R2*. San Diego: Dassault Systèmes BIOVIA Corp.

Hölck, O., Bauer, J., Wittler, O., Lang, K. D., Michel, B., and Wunderle, B., 2011, Experimental Contact Angle Determination and Characterization of Interfacial Energies by Molecular Modelling of Chip to Epoxy Interfaces, *Electronic Components and Technology Conference*, pp. 1079–1085.

Kostoglou, M., and Karabelas, A. J., 1998, Comprehensive Modeling of Precipitation and Fouling in Turbulent Pipe Flow, *Ind. Eng. Chem. Res.*, Vol. 37, pp. 1536–1550.

Leach, A. R., 2001, *Molecular Modelling, Principles and Applications*, 2nd ed., Pearson Education Limited, Essex.

Mwaba, M. G., Golriz, M. R., and Gu, J., 2006, A semi-empirical correlation for crystallization fouling on heat exchange surfaces, *App. Therm. Eng.*, Vol. 26, pp. 440–447.

Pießlinger-Schweiger, S., 2005, Surface treatment of metallic heat exchangers, *Heat Exchanger Fouling and Cleaning - Challenges and Opportunities*, Kloster Irsee, Germany, June 5 – 10, 2005, Engineering Conferences International, Brooklyn, NY, USA.

Puhakka, E., and Lecoq, E., 2015, Organo silicon and titanium oxide coatings for mitigation of $CaCO_3$ depositions, *Heat Transfer Engineering*, Vol. 36, pp. 721-730.

Puhakka, E., Riihimäki, M., and Keiski, R. L., 2008, Fouling mechanisms by *ab initio* calculations – Condensation reactions on the rutile (101) surface and adsorption of ions on the Cr_2O_3 surfaces, *Proceedings of the 7th International Conference on Heat Exchanger Fouling and Cleaning – Challenges and Opportunities*, eds. H. Müller-Steinhagen, M. R. Malayeri, and A. P. Watkinson, ECI Symposium series, Tomar, Portugal, July 1–6,

ISBN: 978-0-9984188-1-0; Published online www.heatexchanger-fouling.com

2007, The Berkeley Electronic Press, Vol. RP5, pp. 300–307.

Sadeghinezhad, E., Kazi, A. B., Badarudin, A., Zubair, M. N. M., Dehkordi, B. L. D., and Oon, C. S., 2013, A review of milk fouling on heat exchanger surfaces, *Rev. Chem. Eng.*, Vol. 29, pp. 169–188.

ISBN: 978-0-9984188-1-0; Published online www.heatexchanger-fouling.com